

# Wide Field Infrared Survey Telescope [WFIRST]: Telescope design and simulated performance

R. Goullioud<sup>\*a</sup>, D. A. Content<sup>b</sup>, G. M. Kuan<sup>a</sup>, J. D. Moore<sup>a</sup>, Z. Chang<sup>a</sup>, E. T. Sunada<sup>a</sup>,  
J. Villalvazo<sup>c</sup>, J. P. Hawk<sup>b</sup>, N. V. Armani<sup>d</sup>, E. L. Johnson<sup>b</sup>, C. A. Powell<sup>b</sup>

<sup>a</sup>Jet Propulsion Laboratory, California Institute of Technology, Pasadena CA, USA

<sup>b</sup>NASA Goddard Space Flight Center, Greenbelt MD, USA

<sup>c</sup>Applied Sciences Laboratory Inc., Baldwin Park CA, USA

<sup>d</sup>SGT Inc, Greenbelt MD, USA

## ABSTRACT

The Wide Field Infrared Survey Telescope (WFIRST) mission concept was ranked first in new space astrophysics missions by the Astro2010 Decadal Survey, incorporating the Joint Dark Energy Mission payload concept and multiple science white papers. This mission is based on a space telescope at L2 studying exoplanets [via gravitational microlensing], probing dark energy, and surveying the near infrared sky. Since the release of the Astro2010 Decadal Survey, the team has been working with the WFIRST Science Definition Team to refine mission and payload concepts. We present the current interim reference mission point design of the payload, based on the use of a 1.3m unobscured aperture three mirror anastigmat form, with focal imaging and slit-less spectroscopy science channels. We also present the first results of Structural/Thermal/Optical performance modeling of the telescope point design.

**Keywords:** WFIRST, Wide Field Imaging, Three Mirror Anastigmat, Telescope, Finite Element Analysis

## 1. INTRODUCTION

Our view of the universe has changed dramatically in recent years. We now know that most of the matter in the universe is invisible, and that the expansion of the universe is accelerating in an unexpected and unexplained way (dark energy). We now know there are many exoplanets, but have not fully determined their frequency or orbital distribution. Ground based experiments are ongoing and more are planned, but the atmosphere limits them: Atmospheric seeing and the limits of adaptive optics technology mean that wide field images are blurred. The near infrared spectrum is largely absorbed by water except for a few spectral windows. Observing transient phenomena (supernovae or exoplanet detections) requires calibration among multiple observatories that are hampered by weather and the circadian cycle. A space telescope with a wide field of view in the near infrared (NIR) spectrum can solve these challenges.

Unlike prior decadal reviews, which chose among well-known candidate mission concepts, the Astro2010 Decadal survey (report: “New Worlds, New Horizons”)<sup>1</sup> ranked the Wide Field Infra-red Survey Telescope (WFIRST) first in new space missions as a combination of the science and hardware concept from the Joint Dark Energy Mission<sup>2,3</sup> (JDEM) with the science agendas of the proposed Microlensing Planet Finder<sup>4</sup> (MTF) and Near Infra-Red Sky Surveyor<sup>5</sup>. WFIRST will take precision images and spectra over thousands of square degrees, with very high image quality and stability greater than that of the Hubble Space Telescope (HST). Since a 50x wider field-of-view (FOV) than Hubble's two-mirror telescope is required, our design uses an unobscured Three Mirror Anastigmat (TMA) design with a 1 square degree FOV. Unobscured TMAs have been flown for Earth-mapping telescopes and in ground telescopes, but not for an astrophysics space telescope. An enabling factor for the mission is the availability of near infrared (NIR) imaging array detectors that can be used to “tile” a large focal plane assembly.

This paper presents the Initial Design Reference Mission (“IDRM”) for WFIRST, emphasizing the telescope design and analysis. As the payload design is, to a large extent, a derivative of the JDEM-Omega payload design<sup>2,3</sup>, we refer to prior publications for its science and payload details. Another more current programmatic reference is the recently completed Interim Report<sup>6</sup> from the science definition team<sup>7</sup> working with the project office. Section 2 describes the current IDRM design. Section 3 describes how the telescope was modeled and the results from the gravity sag and thermal structural analysis.

[\\*renaud.goullioud@jpl.nasa.gov](mailto:renaud.goullioud@jpl.nasa.gov), 818 354 7908, 4800 Oak Grove Drive, Pasadena CA, USA 91109

## 2. INTERIM DESIGN REFERENCE MISSION PAYLOAD

A discussion on the requirements for WFIRST as well as the initial trade study leading to the interim design reference mission can be found in reference<sup>8</sup>. The major change from JDEM-Omega is the switch to an unobscured telescope form. The advantages of this form for dark energy science have been pointed out before<sup>9-11</sup>, and notably includes improved MTF since the large central obscuration for stray light baffles (JDEM-Omega had a 50% linear obscuration) is not needed, improved sensitivity due to no loss of area, and increase in flexibility in design due to the aperture bias that more naturally allows beam clearance. One advantage of the unobscured TMA over the three mirror system without an intermediate focus is the stray light reduction made possible by the placement of a field stop at the intermediate focus, limiting stray light entering the instrument volume. Drawbacks of the unobscured form include a larger overall telescope packaging volume, somewhat tighter alignment tolerances, and potentially more difficult mirror fabrication and alignment. We felt this last point is often overstated when improvements in mirror fabrication and alignment tooling are taken into account. For example, the Landsat data continuity mission/operational land imager (LDCM/OLI) instrument is an unobscured, wide field of view four mirror system, and has been reported as having no problems or delays during fabrication and alignment<sup>12</sup>.

### 2.1 IDRM description

Figure 1 shows the field-of-view layout, along with views of the FOV layouts of the James Webb Space Telescope (JWST) as planned and the current HST instrument complement FOV. In addition, we include the moon as seen from earth for an idea of scale on the sky. Each square in the figure is a 4Mpix HgCdTe NIR detector array. However the pixel sizes are much coarser than those of the facility cameras on HST or JWST, as appropriate for a mission emphasizing wide surveys over pointed deep observations. Overall the imaging etendue (aperture area product with field of view area) is greater than ten times that of HST/WFC3 or JWST/NIRCAM. Compared to the JDEM-Omega concept, the total pixel count is preserved, but two NIR arrays are moved from each spectroscopy channel (SpC) to the imaging channel (ImC), such that the imaging mosaic increases from 6x4 to 7x4. The FOV loss with pixels in the spectrometers is compensated by a larger focal length ratio, increasing from roughly 2:1 in JDEM-Omega to 2.5:1 here. The SpC field area is then as large as in JDEM-Omega.

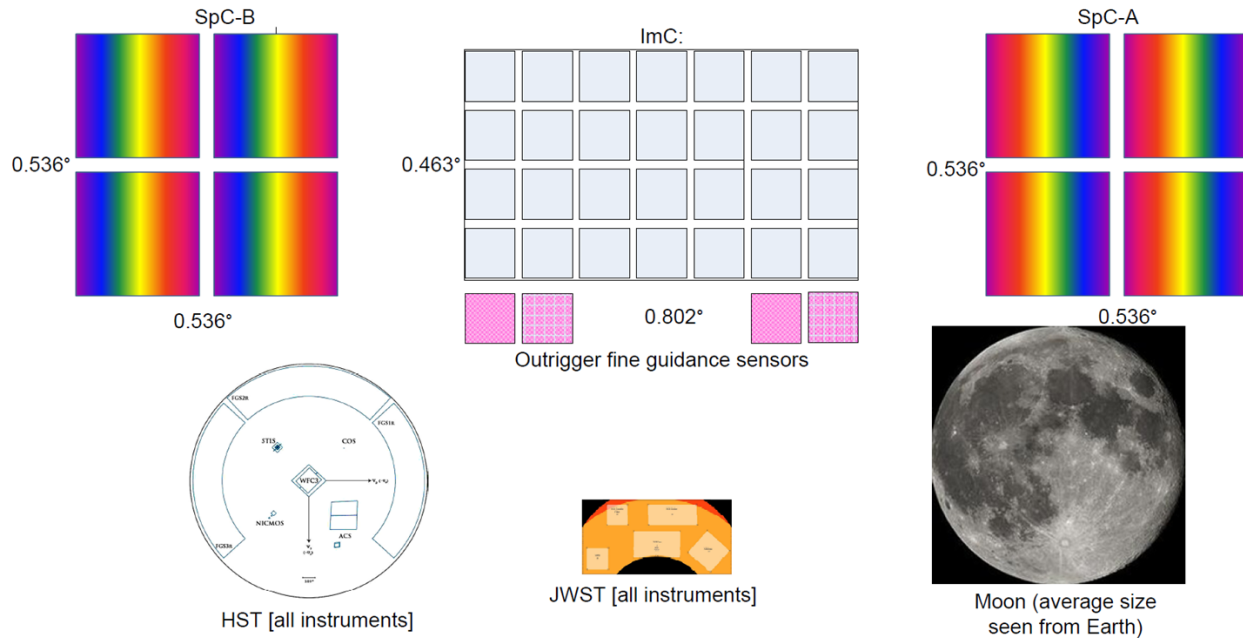


Figure 1. Field of view diagram for the WFIRST interim design reference mission (top row). Each square is a 4Mpix HgCdTe array; different sizes denote differing pixel scales. SpCA & B are at right and left, ImC is centered in the field. Outrigger fine guidance channels are also in the ImC optical train and focal plane. An auxiliary guider (not shown) is available when the supernova prism is selected via the filter wheel, placing a spectrum on the outrigger guidance sensors. Bottom Row: to-scale views of JWST & HST fields of view and the full Moon.

Figure 2 (left) shows a ray trace of the f/15.9 imaging instrument. The unobscured TMA is folded after the aberrated intermediate focus. The tertiary mirror and subsequent fold mirrors are placed behind the primary mirror to be close to the mechanical load path from the telescope to the spacecraft, for maximum stability. A filter wheel is located just after the telescope exit pupil, which acts as the thermal/mechanical/optical interface between the telescope and imaging channel. The focal plane is located opposite the sun-illuminated side so it can be placed close to a passive radiator.

Similarly, Figure 2 (right) shows the two spectroscopy channel ray traces, the two channels being mirror images with dispersion directions opposed 180° on the sky to help disentangle overlapping spectra. Two fold mirrors straddle the intermediate (Cassegrain-like) focus so that the spectrometer ray bundles clear that of the imaging channel and are moved outside the ray bundle coming from the secondary mirror. The beam returning from the tertiary is folded away from the sun-illuminated side of the observatory. The spectrometer itself consists of a 3-prism group (zero deviation or direct vision prism) and a 4-element Shapley lens. The beam entering the prism group is still f/15.9 and is reduced to f/6.9 by the Shapley lens. Each group's final surface has a mild conic, otherwise all instrument surfaces are spherical. All elements are vacuum-spaced for operation at ~170K. In the imaging channel one of the elements in the filter wheel is a low resolving power ( $R \geq 75$ ) focal prism, used for spectroscopy of SN1a.

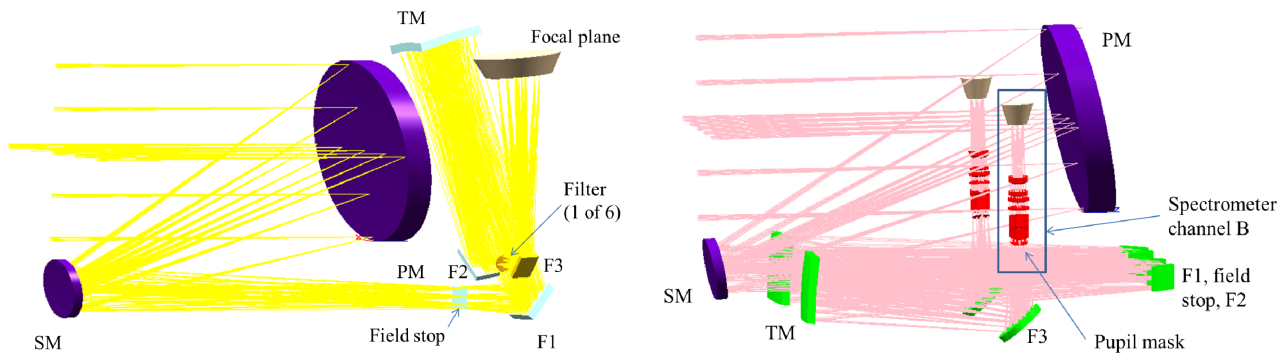


Figure 2. Left: Ray trace of the Imaging Channel. ImC is an unobscured 1.3m three mirror anastigmat with a single fold between the intermediate focus and the tertiary, and two additional fold mirrors on either side of the exit pupil. The feed optics (non-common telescope fold mirrors and tertiary mirror) and instrument (pupil mask, filter, and fold mirror) are packaged behind the primary mirror for stability. Right: Ray trace of the Spectrometer Channels. The primary and secondary mirrors are shared with the ImC channel. SpC use two fold mirrors on either side of the intermediate focus and a third fold mirror before the exit pupil to allow the instrument barrel to be located outside the telescope main barrel with the focal plane on the cold side of the observatory. The two spectrometer channels A (far side and B (near side) are mirror images. In both images the sun direction is towards the bottom of the page and the cold side on the observatory on the top.

Overall performance margins are improved relative to the JDEM-Omega design. We set as a rule of thumb a minimum of a factor of two between the overall required wavefront allocation and that at the worst field-wavelength combination for a given channel. The ImC has a uniform error, ranging from 12 to 19nm over the field including the outrigger fine guidance channels and the science field. As a comparison, the telescope wavefront budget error allocation beyond this design residual is ~57nm rms. Both spectrometer channel designs have additional margin beyond the factor of 2 minimum. Overall this design achieves higher sensitivity, lower noise, and therefore up to twice as short an integration time to the same signal to noise level as compared to the JDEM-Omega design.

## 2.2 Observatory brief description

The payload is designed with stray light control for an observatory that must observe most of the sky over its lifetime. The supernova measurements are made towards the galactic poles for minimal background. Conversely the exoplanet measurements are made looking at the galactic central bulge with a high star density. The IR survey looks both at high galactic latitudes along with a dedicated look in the galactic plane. The galaxy survey measurements will be initially done at high galactic latitudes, working closer to the galactic and ecliptic planes as time permits. Therefore we oriented the unobscured telescope so that the opening in the telescope tube between the primary and secondary mirrors is facing away from the solar vector so that a full wall of ring baffles can be used to block any diffracted light. A large solar array/thermal shroud surrounds the optical and metering components so that no direct sunlight illuminates them for any field of regard.

The three tertiary mirrors are almost identical, as different apertures of the same parent conic mirror. All three instrument channel interfaces from the telescope are focal  $f/15.9$  pupils of similar size and so can be tested using common equipment. Figure 3 is a CAD view of the observatory. This view shows the solar array/thermal shroud which keeps sunlight off the payload throughout its field of regard. The only deployable element is an aperture cover in front of the primary telescope tube (not shown).

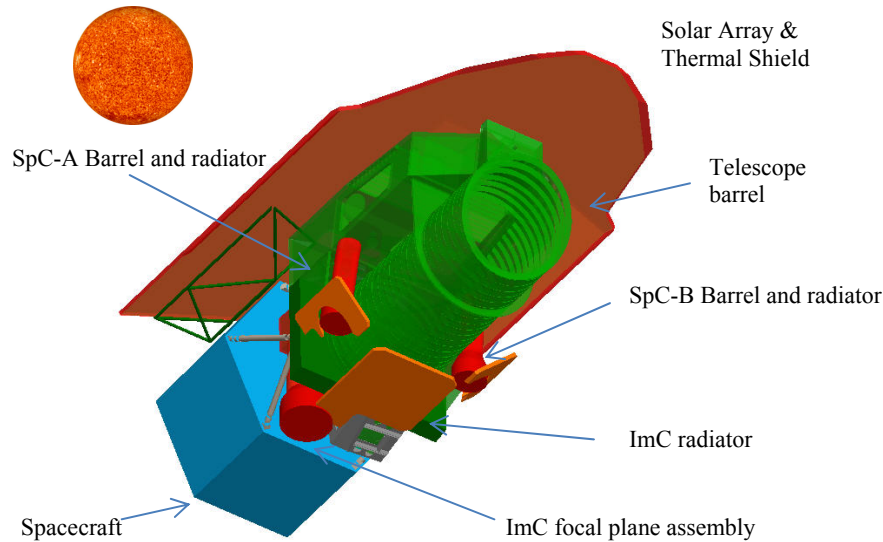


Figure 3. Observatory CAD view, looking from the anti-Sun side. Focal planes and radiators are placed facing anti-Sun and the Solar Array structure/thermal shroud shadows the payload to allow passive cooling. Each instrument channel mounts separately to the telescope structure.

### 2.3 Telescope Mechanical Design

The design of this large off-axis telescope presented several challenges, particularly the use of large rectangular glass mirrors maintaining  $\lambda/50$  figure at low temperatures, and the need for stray light baffling. Weight limits and first mode stiffness dictated a carbon fiber structure where each and every part contributed to stiffness as much as possible while meeting other demands such as baffling and mounting interfaces.

Extremely detailed structural design was required to meet first mode requirements. Maintaining 1-micron diffraction limited quality mirrors at low temperatures (220K) demanded a careful balance of bipod design and determining an adhesive stiffness which was high enough to maintain mirror modes and low enough not to distort the mirror at low temperatures. Commonly used adhesives are too stiff to achieve diffraction limited quality, especially when we are designing for an operating temperature near 200K. The 17.8Hz first mode was achieved primarily through the use of a large, carefully designed "Strongback" box-like structure to which the spacecraft is directly connected by kinematic bipods having titanium cross-blade fittings bonded to each end of a carbon fiber tube. This Strongback structure contains numerous ribs which enhance stiffness and provide convenient places to mount rectangular mirrors. It is designed to give access to mirrors and reduce acoustic loading stress by means of large holes in the sides. Figure 4 (left) shows the detailed mechanical (CAD) model of the telescope.

A five axis, athermal secondary mirror actuation system capable of 3mm range and 3micron positioning was designed. It uses stepper motors without micro-stepping, which allows them to be turned off so that motor power or heat is not an issue. The primary mirror and mounts are nearly identical to those of the Kepler primary mirror, and therefore relies on the excellent overall performance and heritage of that successful observatory.

The telescope design has had only a cursory check of launch stresses with an emphasis on achieving first mode requirements and minimizing adverse mirror mounting effects. However a design that achieves the highest first modes is structurally efficient by definition, and therefore launch stresses are generally low, requiring minor low-mass reinforcements where stress concentrations are seen in a full up finite element analysis.

Simple bipods having 2-D shapes (i.e. cut from titanium or other plate stock) were designed to reduce cost. This design does not lend itself well to the use of Invar alone, so instead an Invar pad is used between the glass and the titanium bipod. A lay-up carbon-fiber design should be investigated to possibly eliminate the Invar pad and reduce the effect of an "inverted" titanium bipod on the mirror figure. Analysis shows the titanium bipods in the current model do work well enough down to about 220K. Relatively thick bonds were employed for mirror mounting in the structure because carbon fiber structures do not lend themselves to machining of interface surfaces. If the structure ribs where mirrors mount can be jiggled to 1/3mm or better, no interface machining would be required.

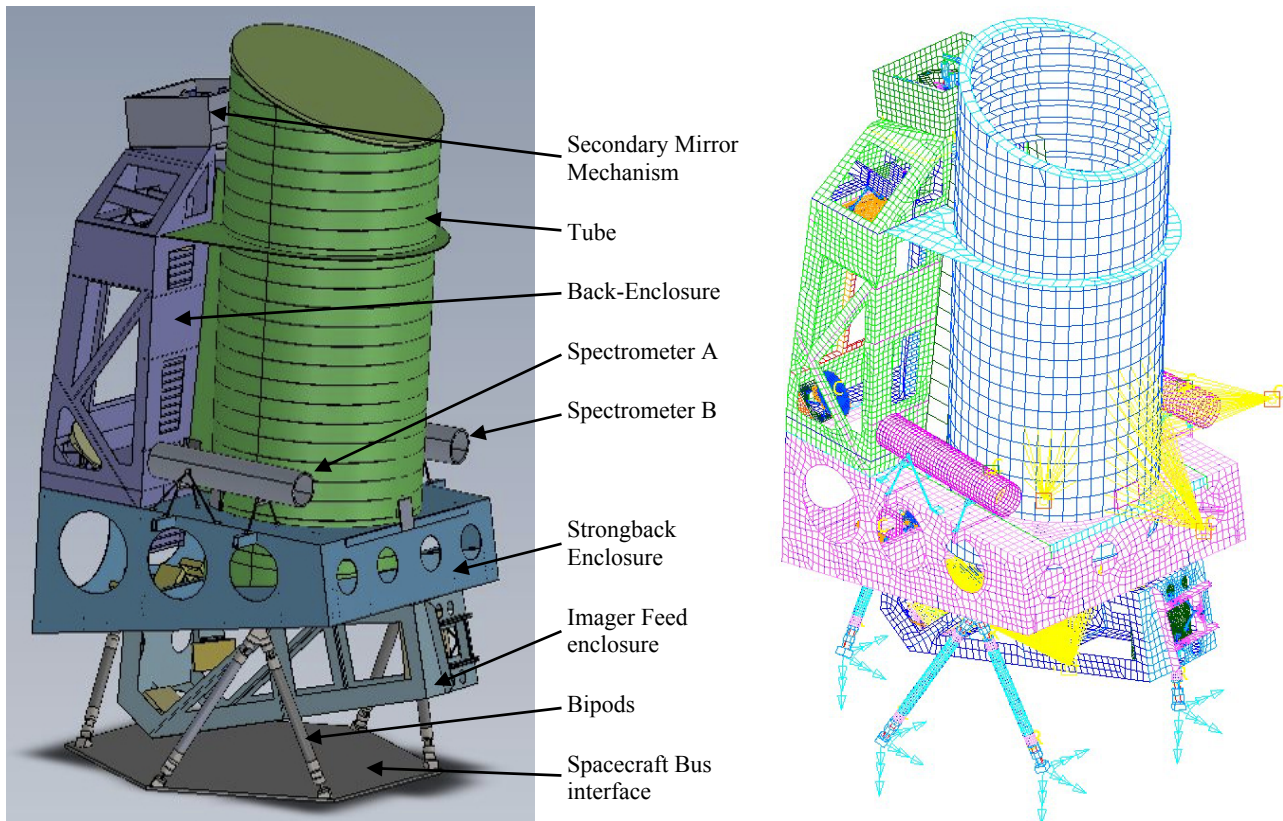


Figure 4. (left) Telescope mechanical model and (right) telescope finite element model that includes 209,748 elements.

### 3. TELESCOPE MODELING AND ANALYSIS

#### 3.1 Structural Finite Element Modeling

The preliminary design of the telescope meets both survival and performance requirements. These requirements include meeting minimum fundamental frequencies in lateral and axial directions, surviving maximum launch loads, as well as requirements for jitter, sinusoidal vibration, acoustics, and more. From an optical point of view, the design shall meet the optical performance requirements after being exposed to the absence of gravity and on-orbit thermal environments.

Nastran models were constructed to perform finite element analysis (FEA) of the preliminary design of the telescope. The commercially available IDEAS NX software tool<sup>13</sup> was used as the pre- and post-processor. The models were verified by NASA standard procedures, including checks on element geometry, grounding, maximum diagonal ratio, Nastran Epsilon, unit gravity constraint loads, free-free modal, common CTE, etc. After several iterations of design changes and finite element analysis, the STOP-ready (Structural/Thermal/Optical Performance ready) version of the telescope FEA model weighs in at 1,139kg with contingency, and has 103,219 nodes and 209,748 elements. Figure 4 shows the FEA model of the telescope (right figure) next to the mechanical model of the telescope.

The first analysis performed on the STOP model was modal analysis with proper boundary conditions prescribed at the Spacecraft/Telescope interface. The analysis predicted the frequency of the fundamental lateral mode to be 17.8Hz,

which exceeds the minimum requirement plus a 15% margin. First resonant mode of each optic was then identified and the frequencies recorded. Next, the model was sent to the thermal analyst to perform temperature mapping from the thermal model to the structural model. Some of the optics experienced high surface deformation under the operational thermal environment. To improve the optical performance, more detailed stand-alone models of several optics were constructed, including the primary, the secondary, the tertiary, and two fold mirror subassemblies. It was found that the surface deformations were primarily attributed to the CTE mismatch between the mirror (made of ultra-low expansion (ULE) fused silica) and the supporting titanium bipods, as well as the attachment locations of the bipods. After introducing Invar bond-pads between the mirror and the titanium bipods, and the relocating some of the bipods, the surface deformations were reduced to an acceptable level.

Jitter analysis will be performed on the integrated spacecraft/telescope model. The telescope structural model has been sent to the project office for integration with the spacecraft model for jitter analysis.

### 3.2 Thermal design and modeling

The thermal point design takes a hybrid approach. Most of the optics are thermally controlled with a dedicated heated enclosure. In some cases, multiple heater zones are employed per optic based on engineering judgment. Heating occurs via radiation with feedback sensors on the optic. In addition, the point design retains active heating of the structure to maintain acceptable amounts of rigid-body motion and for hardware safety purposes. In some areas, such as the Feed Enclosure, heating of the structure will serve the dual purpose of rigid-body motion control as well as surface figure error control of the optics. In these cases, dedicated optics heaters will not be employed.

A thermal math model (TMM) of the latest WFIRST telescope CAD geometry was developed using the commercially available software tool Thermal Desktop<sup>14</sup>. The TMM includes the telescope structure, optics and a TMM of the spacecraft bus solar arrays and spectrometers. The TMM has sufficient level of detail with approximately 12500 nodes and 9000 surfaces, including 1104 nodes and 1816 surfaces for the primary mirror, and 296 nodes and 294 surfaces for the secondary mirror. Figure 5 (left) shows the thermal model of the telescope while Figure 5 (right) shows the predicted temperature map of the telescope. As expected the telescope temperature ranges from the hot sunshield/solar array internal panel at more than 360K to the cold radiators at less than 100K. Most of the telescope structure is kept at 220K using 205Watts of heating power with the exception of the telescope tube that is not thermally controlled.

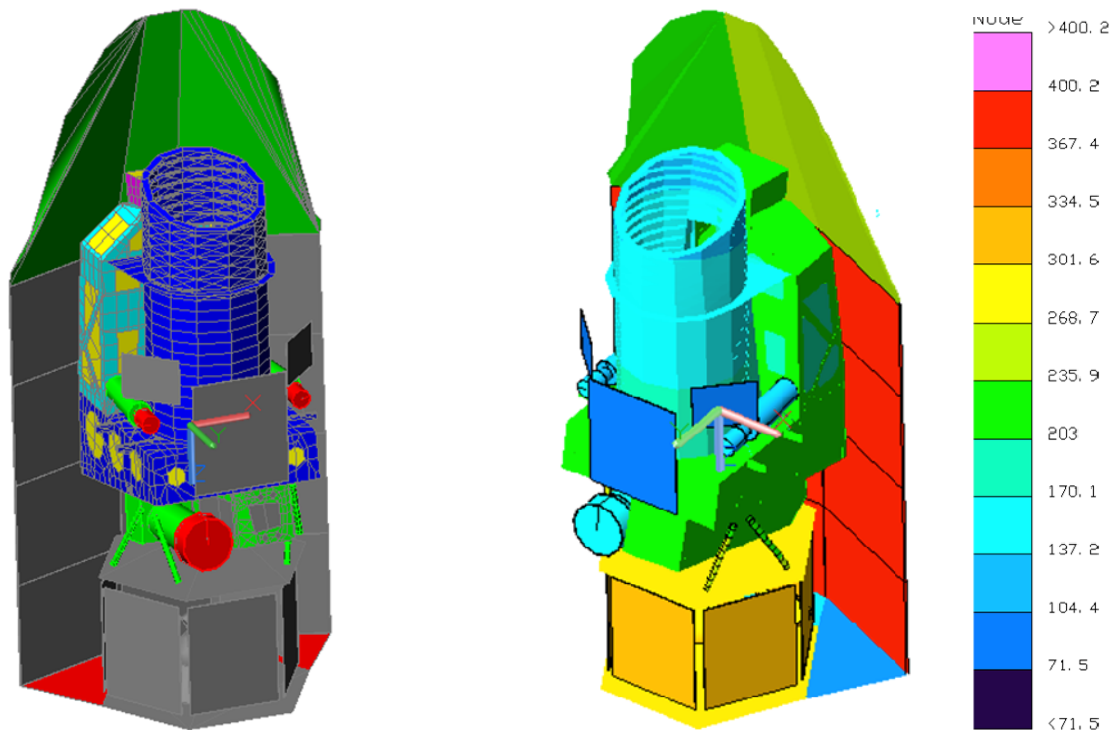


Figure 5. Telescope thermal model (left) and telescope predicted temperature map (in Kelvins) (right).

### 3.3 Optical Modeling:

The commercially available Zemax software tool<sup>15</sup> was used for the WFIRST IDRMM telescope optical design, tolerancing, and end-to-end performance analysis. Optical modeling includes optical performance analysis of on-orbit gravity off-loading, on-orbit thermo-elastic rigid-body shift, and on-orbit thermo-elastic surface deformation. Optical performance analysis of surface deformation due to gravity off-loading is currently in progress. In all of these cases, only the Imaging channel was modeled. By the time STOP analysis of the IDRMM was ready to proceed, new DRM designs that no longer include the two spectrometer channels were proposed, and therefore no STOP analysis for these channels were conducted.

The on-orbit, actively controlled, compensator of the IDRMM is the secondary mirror of the TMA. With five degrees-of-freedom (DOF) adjustment, it is situated at a location of high sensitivity and can compensate for misalignments and, to limited extent, shape deformations of most of the optics.

On the ground, two compensators are required, one being the secondary mirror with a second compensator used to aim the beam at the center of the exit pupil of the telescope. The F2 fold mirror (see Figure 2, left) was selected to include a 5 DOF mount design that would allow for sub-micron level manual adjustments.

Telescope alignment on the ground adheres to the policy of minimal complexity and low cost. Since an actuated compensator, the secondary mirror mechanism, is already included in the design, we decided to take advantage of its large range of motion as part of the ground alignment process. Allowing for a liberal 150um 1-sigma mechanical placement accuracy of all optics, it is found that the secondary mirror and an additional manual compensator, the F2 fold mirror, are all that is needed to maintain high optical performance and minimize labor-intensive, precision alignment. Furthermore, fiducials on each optic allow for precision determination of the position and orientation of the optics, which in turn simplifies modeling of the as-built telescope to determine the corrections needed to optimize the telescope performance.

### 3.4 Ground to Orbit Gravity Sag analysis:

On-orbit gravity off-loading of the telescope is always a concern. There have been numerous methods documented in the literature<sup>16-17</sup> as to how to compensate for gravity during on-ground alignment. However, the simplest method is to have a design that is forgiving enough as to not require any gravitational compensation on the ground. With this in mind, the IDRMM structure was designed to be sufficiently stiff as to not deform much in the presence of gravity, while any remaining misalignment due to gravity can be compensated using the secondary mirror. This design was then modeled with and without the effect of gravity on the rigid-body position of each optic. Rigid-body position perturbation data was obtained from the output of the finite element model when a gravitational force is applied. These perturbations were then applied to the optical model in Zemax, and the resulting optical performance over the field-of-view was evaluated. Performance was then optimized by adjusting the secondary mirror in 5-DOF.

In the optical model, the IDRMM imager channel over the entire FOV performed with an average wavefront error (WFE) of 15nm RMS. With the gravity sag rigid-body perturbations, the optical performance degraded to 311nm RMS. However, after secondary mirror compensation, the performance returned to 15nm RMS. The optical performance model has shown that the secondary mirror alone can compensate for the effect of gravity on optical alignment.

### 3.5 Structural/Thermal/Optical Performance analysis:

#### *Ground to Orbit Thermo-Elastic Rigid-body Sag:*

Similar perturbation data is applied to the optical model using the output of thermo-elastic rigid-body perturbations due to transitioning from room temperature to the nominal operating thermal environment with a temperature set point of approximately 220K for the telescope optics. Again, the resulting optical performance over the imager FOV is evaluated before and after the perturbations are applied and also with secondary mirror compensation.

In the optical model, the IDRMM imager channel over the entire FOV performed with an average wavefront error (WFE) of 15nm RMS. With thermo-elastic rigid-body perturbations, the optical performance degraded to 514 nm RMS. However, after secondary mirror compensation, the performance dropped back down to 15 nm RMS. Again, the optical performance model has shown that the secondary mirror alone can compensate for much of the thermo-elastic rigid-body perturbations of each optic.

### Ground to Orbit Thermo-elastic Surface Deformation:

In addition to rigid-body motion, a thermo-elastic surface deformation analysis of the IDR design was conducted. The output temperature map from the thermal model of the IDR in the on-orbit nominal orientation was applied to the finite element model. Figure 6 shows the results for the primary mirror. The surface deformation of each optic was generated and the resulting data was applied to the optical model in Zemax using a Zernike decomposition of the surface deformations. Seventy-five Zernike polynomial coefficients were applied. Again, the optical performance was evaluated before and after compensation using the secondary mirror. As expected, the secondary mirror compensator has little or no influence over higher order terms, but does have influence over defocus as well as astigmatism and coma to a lesser extent.

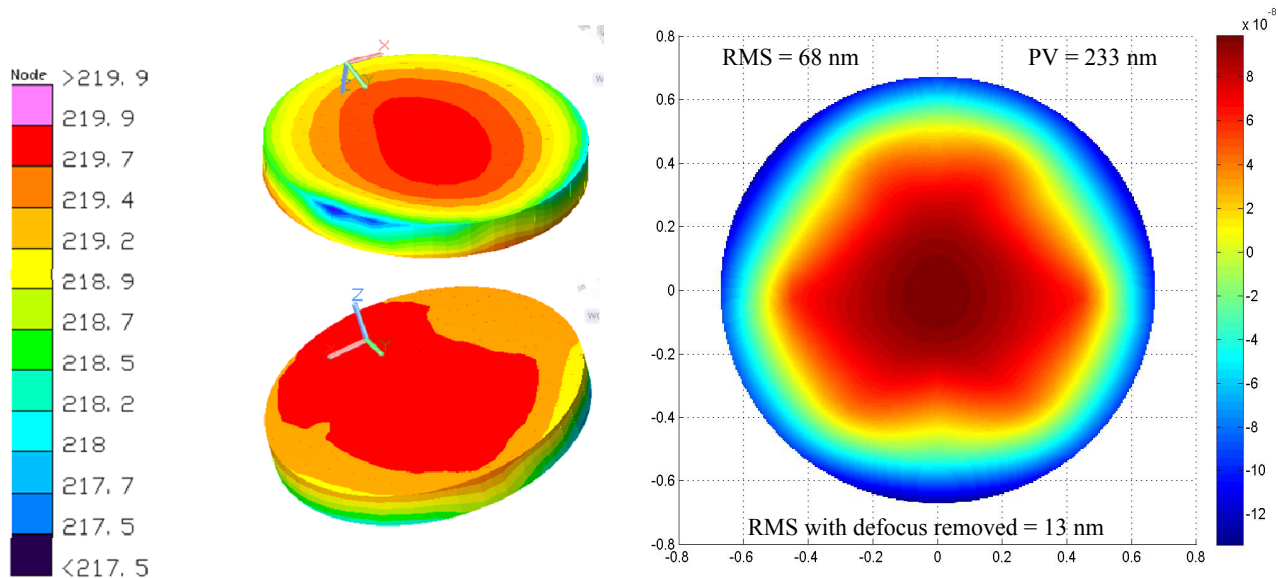


Figure 6. (left) Primary mirror temperature map (in Kelvins) and (right) primary mirror surface error map. The mirror average temperature is 219.8K, very closed to the 220K target. Using multiple heater zones the thermal gradient is kept below 2.5K. The dominant term in the predicted surface error for the primary mirror is defocus. This term can easily be removed by on-orbit realignment of the telescope. The surface error is mostly produce by the mirror mount that is not athermal over the 70K range from room temperature to the operating temperature.

Once again, the nominal WFE of the IDR is 15nm RMS. With thermo-elastic surface deformations, the optical performance degraded to 61nm RMS. After secondary mirror compensation, the performance recovered only to 47nm RMS. Unlike rigid-body misalignments, surface deformations do include higher order Zernike components that a rigid-body compensator cannot counteract. As such, more of the wavefront error remains.

The chart in Figure 7 shows the total RMS wavefront error and the contribution of Zernikes 4 through 20 at the center of the imager FOV. The coefficients follow the Noll ordering. Compensation with the secondary mirror does reduce the effects of Zernikes 4, 5, and 6 (defocus and astigmatism), though it has little effect on any terms above 8. Zernike coefficients 7 and 8 (coma) actually increased after compensation, though this is likely due to optimization over the entire FOV rather than only at a single field point.

### 3.6 Thermal Stability analysis:

One question that arises for the measurement which seems to require the most stringent system stability performance, weak gravitational lensing, is why we would expect our system to be more stable than the (much more expensive) Hubble Space Telescope (HST). We investigated the actual stability of the HST and compared it to our requirements as we understand them. As an example of the systematic error limits achieved to date with HST weak lensing observations we cite the COSMOS work<sup>18</sup> with an uncertainty in the systematic ellipticity of 0.01 when we expect to need <math>< 0.001</math> or better for WFIRST.

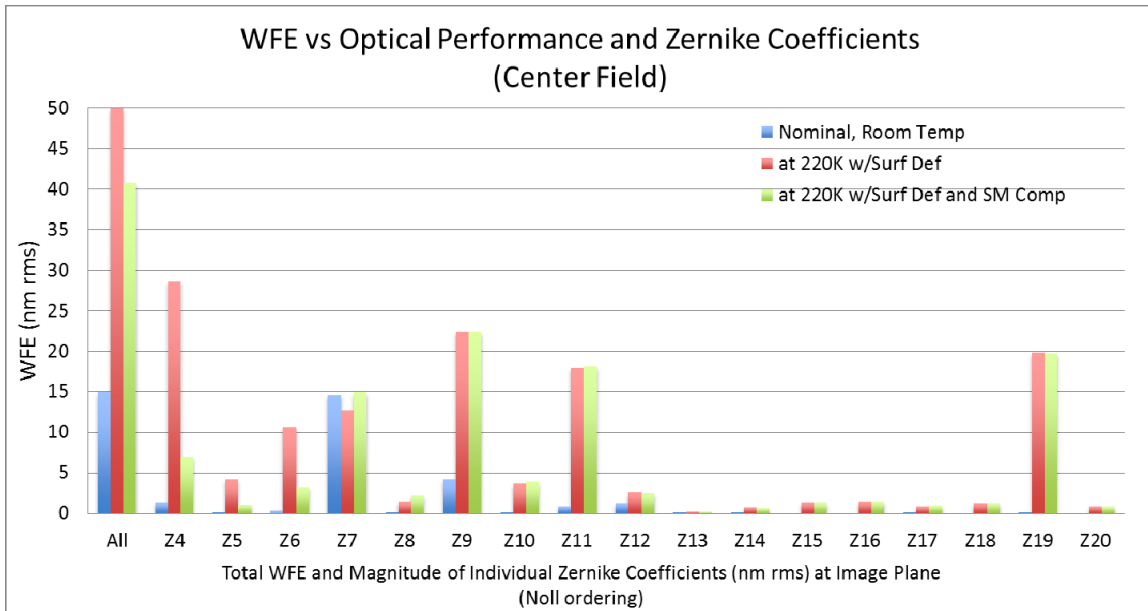


Figure 7. Optical wave-front error with Zernike decomposition for all the telescope optics for 3 conditions: nominal condition after telescope alignment at room temperature, surface deformation from temperature shift to 220K and surface deformation after telescope realignment at 220K using secondary mirror compensation.

The HST is in low Earth orbit, and has an operational requirement that when targets are obscured by the Earth, HST remains 3 axis stabilized in that orbital attitude, so that earth light enters the aperture. Therefore, not only does the HST have earth thermal loading alongside the telescope during science integrations, but the thermal sink temperature of the aperture varies from cold deep space to night or daytime Earth temperatures. As documented in STScI reports<sup>19-20</sup>, this behavior is now well understood empirically. The structure in HST metering the primary mirror to the secondary mirror is 4.9m long, and has changes in axial gradient (the dominant term in the 'breathing' of HST focus) of 5°C. In addition, the effective CTE of the metering structure can be inferred from the empirical breathing model as follows: The coefficient of defocus is 0.81  $\mu\text{m}/^\circ\text{C}$  where the motion is in linear units of movement of the secondary mirror. Including the metering distance, one infers an effective CTE of 0.165ppm/°C. This is about 4 times the material CTE of 0.045ppm/°C, and significantly larger than modern structural composites used at their design temperature.

For WFIRST each of these factors is less sensitive (CTE, metering distance, and secondary mirror magnification), reducing the defocus we can expect. As an example of what the combination of improved materials and the improvements that could be expected from a higher orbit that never puts the Earth in the aperture, we examined the case of the Chandra telescope<sup>21</sup>. Chandra has no worse than 0.2degree gradients and has material with lower CTE. This is of order 50x or greater improvement in thermo-optical stability. This improvement suggests that a design of materials and thermal control similar to Chandra should suffice for thermal stability.

Using the FEA model, we analyzed the optical wavefront change for the IDRM for two spacecraft positions. The nominal position had the Sun behind the sunshield (the Sun angle being normal to the sunshield) while in the second orientation the Sun angle was tilted by 10 degrees in Roll and 30 degrees in Pitch. Figure 8 shows the temperature change for the primary mirror (left figure) and the corresponding change in the mirror surface error (right figure). Indeed, from the benign environment at L2, the optics temperature can be maintained to a few tens of milliKelvins. The change in the mirror temperature is small (about 50milliK) and the resulting change in wavefront significantly below a single nanometer. Similar results were observed with the other mirrors in the optical train.

Although we have yet to complete optical performance modeling of this thermal transient case, we can infer much from the surface deformation optical performance analysis already completed. In that case, the modeled thermo-elastic deformation due to a bulk temperature drop of 53K produced an additional 63nm RMS on the primary mirror, 50nm RMS on the secondary mirror, 74nm RMS on fold mirror 1, 22nm RMS on the tertiary mirror, and 34nm RMS on fold mirror 2. When these surface deformations are applied to the optical model (for a total RSS surface figure error of 116.5 nm RMS), without compensation, the resulting wavefront error increased from 15nm RMS to 61nm RMS.

However, transient analysis shows that reorienting the observatory by 10 degrees of roll and 36 degrees of pitch produce surface error changes of 62 picometers RMS for the primary mirror, 55 pm RMS for the secondary mirror, 14 pm RMS for the tertiary mirror, 68 pm RMS for fold mirror 1, and 231 pm RMS for fold mirror 2 for an RSS total of 255 pm RMS. We expect that this amount of additional optical surface deformation to have a negligible effect on the optical performance in this extreme orientation.

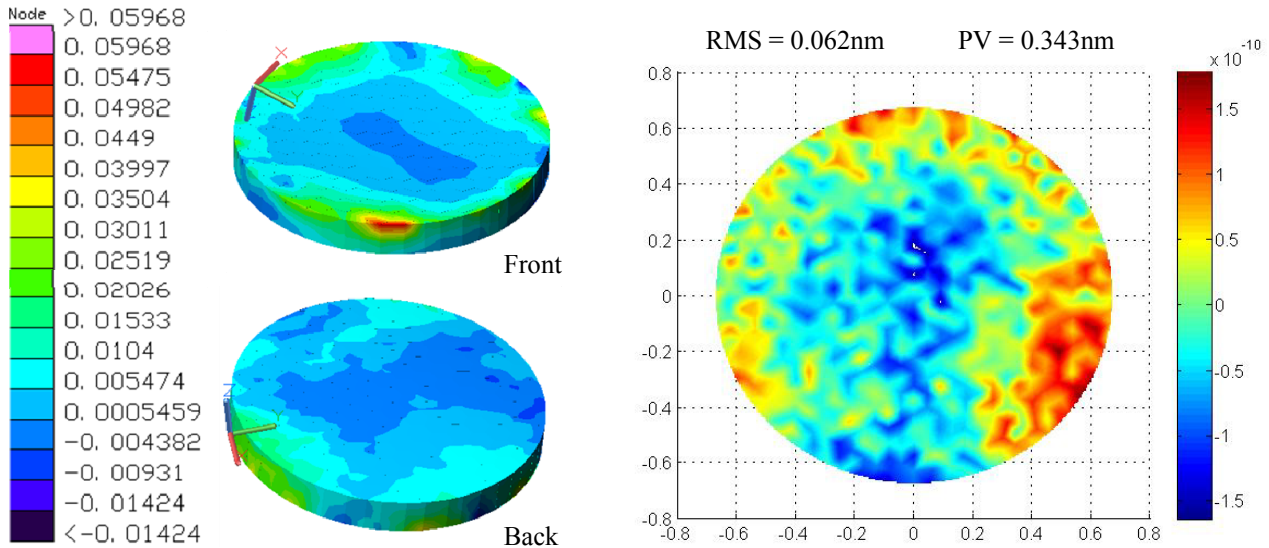


Figure 8. Primary mirror temperature change (in Kelvins) and primary mirror surface error map change.

On the other hand, rigid-body motion due to thermal transients when slewing between the nominal orientation to the extreme orientation does produce a noticeable effect. As discussed previously, the secondary mirror can compensate for all of the wavefront errors due to thermo-elastic rigid-body motions between ground and orbit. In addition, thermal transient analysis of the telescope for the case of an extreme slew (10deg roll, 36deg pitch) shows that additional rigid-body motions of the optics degrades optical performance from 15nm RMS to 18nm RMS – a statistical addition of 10 nm RMS. Although this is not negligible, it is nevertheless small enough to consider not having to apply secondary mirror corrections to optimize telescope performance following large observatory slews. That said, if secondary mirror compensation were applied, it is expected that all of the additional wavefront error will be negated.

#### 4. SUMMARY

Overall this interim design performs well and is ready to proceed into detailed study and build phases. Results from initial STOP analysis show all telescope requirements can be met using a classic design for “room” temperature application, brought down to 220K. The five degrees of freedom mechanism at the secondary mirror appears to be sufficient for on-orbit realignment of the telescope. The team recommends the development of one engineering model of a mirror mount to validate this analysis. In addition, if time and cost permit, the team recommends development of a 2-D bipod fabricated from a carbon-fiber composite material lay-up that could significantly reduce surface deformation of optics operating down to 200K.

#### 5. ACKNOWLEDGMENTS

The research described in this presentation was performed at the Jet Propulsion Laboratory of the California Institute of Technology, under contract with the National Aeronautics and Space Administration, in close collaboration with the WFIRST project team at the NASA Goddard Space Flight Center.

## REFERENCES

- [1] Astro2010 final report: [http://www.nap.edu/catalog.php?record\\_id=12951](http://www.nap.edu/catalog.php?record_id=12951)
- [2] JDEM input to Astro2010: [http://wfirst.gsfc.nasa.gov/science/astro2010\\_rfi/Astro2010\\_JDEM-Omega\\_RFI.pdf](http://wfirst.gsfc.nasa.gov/science/astro2010_rfi/Astro2010_JDEM-Omega_RFI.pdf)
- [3] D. A. Content, M. G. Dittman, B. Firth, J. M. Howard, C. E. Jackson, J. P. Lehan, J. E. Mentzell, B. A. Pasquale and M. J. Sholl, "Joint Dark Energy Mission optical design studies", Proc. SPIE 7731, 77311D (2010); <http://dx.doi.org/10.1117/12.859144>
- [4] MPF input to Astro2010: <http://arxiv.org/abs/0902.3000>
- [5] NIRSS input to Astro2010: [http://wfirst.gsfc.nasa.gov/science/astro2010\\_rfi/Astro2010\\_NIRSS\\_RFI.pdf](http://wfirst.gsfc.nasa.gov/science/astro2010_rfi/Astro2010_NIRSS_RFI.pdf)
- [6] SDT interim report: [http://wfirst.gsfc.nasa.gov/science/WFIRST\\_IDRM\\_Report\\_Final\\_signed\\_Rev1.pdf](http://wfirst.gsfc.nasa.gov/science/WFIRST_IDRM_Report_Final_signed_Rev1.pdf)
- [7] Science definition team for WFIRST membership: [http://wfirst.gsfc.nasa.gov/science/sdt\\_membership.html](http://wfirst.gsfc.nasa.gov/science/sdt_membership.html)
- [8] D. A. Content, R. Goullioud, J. P. Lehan, J. E. Mentzell, "Optical design trade study for the Wide Field Infrared Space Telescope [WFIRST]", Proc. SPIE 8146, 81460Y (2011); <http://dx.doi.org/10.1117/12.898528>
- [9] Gil Moretto, Maud P. Langlois and Marc Ferrari, "Suitable off-axis space-based telescope designs", Proc. SPIE 5487, 1111 (2004); <http://dx.doi.org/10.1117/12.548893>
- [10] Kuhn, J. R., Hawley, S. L., "Some Astronomical Performance Advantages of Off-Axis Telescopes," PASP 111 759 601-620 (1999).
- [11] Michael L. Lampton, Michael J. Sholl and Michael E. Levi, "Off-axis telescopes for dark energy investigations", Proc. SPIE 7731, 77311G (2010); <http://dx.doi.org/10.1117/12.856500>
- [12] Michael G. Dittman and Brenda Firth, "OLI telescope post-alignment optical performance", Proc. SPIE 7807, 780705 (2010); <http://dx.doi.org/10.1117/12.860869>
- [13] I-DEAS NX, Siemens PLM Software, [http://www.plm.automation.siemens.com/en\\_us/products/nx/](http://www.plm.automation.siemens.com/en_us/products/nx/)
- [14] Thermal Desktop, C&R Technologies Inc., <http://www.crtech.com/thermaldesktop.html>
- [15] Zemax 12, Radiant Zemax LLC, <http://www.radiantzemax.com/en/design/home.aspx>
- [16] E. E. Bloemhof, J. C. Lam, V. A. Ferial, and Z. Chang, "Extracting the zero-gravity surface figure of a mirror through multiple clockings in a flightlike hexapod mount", Applied Optics, Vol. 48, Issue 21, pp. 4239-4245 (2009); <http://dx.doi.org/10.1364/AO.48.004239>
- [17] John W. Zinn and George W. Jones, "Kepler primary mirror assembly: FEA surface figure analyses and comparison to metrology", Proc. SPIE 6671, 667105 (2007), <http://dx.doi.org/10.1117/12.732667>.
- [18] Jason D. Rhodes, Richard J. Massey, Justin Albert, Nicholas Collins, Richard S. Ellis, et al., "The Stability of the Point-Spread Function of the Advanced Camera for Surveys on the Hubble Space Telescope and Implications for Weak Gravitational Lensing," Ap J. Supp., 172:203-218, (2007).
- [19] Di Nino, D., Makidon, R. B., Lallo, M., Sahu, K., Sirianni, M., and Casertano, S, "HST Focus Variations with Temperature," Instrument Science Report ACS 2008-03, <http://www.stsci.edu/hst/acs/documents/isrs/isr0803.pdf>
- [20] Colin Cox and Sami-Matias Niemi, "Evaluation of a temperature based HST Focus Model," Instrument Science Report TEL 2011-01, <http://www.stsci.edu/institute/org/telescopes/Reports/ISR-TEL-2011-01.pdf>
- [21] Gary Matthews and Keith Havey, Jr., "Ten years of Chandra: reflecting back on engineering lessons learned during the design, fabrication, integration, test, and verification of NASA's great x-ray observatory", Proc. SPIE 7738, 77380Y (2010); <http://dx.doi.org/10.1117/12.858268>